DER MATERIALS QUARTERLY PROGRESS REPORT

For the Period
July 1, 2003 to September 30, 2003

Prepared by:

David P. Stinton, Manager, and
Roxanne A. Raschke
DER Materials Research
Oak Ridge National Laboratory

For:

Department of Energy
Office of Distributed Energy

DER MATERIALS QUARTERLY PROGRESS REPORT

July—September 2003

TABLE OF CONTENTS

Introduction

RECUPERATORS

Advanced Alloys for High Temperature Recuperators
P. J. Maziasz, B. A. Pint, R. W. Swindeman, K. L. More, and M. L. Santella
Oak Ridge National Laboratory, Oak Ridge, Tennessee

Recuperator Alloys – Composition Optimization for Corrosion Resistance
B. A. Pint
Oak Ridge National Laboratory, Oak Ridge, Tennessee

Recuperator Materials Testing and Evaluation
E. Lara-Curzio
Oak Ridge National Laboratory, Oak Ridge, Tennessee

CERAMIC RELIABILITY FOR MICROTURBINE HOT-SECTION COMPONENTS

Reliability Evaluation of Microturbine Components
H-T Lin, M. K. Ferber, and T. P. Kirkland
Oak Ridge National Laboratory, Oak Ridge, Tennessee

Long-Term Testing in Water Vapor Environments
M. K. Ferber and H-T Lin
Oak Ridge National Laboratory, Oak Ridge, Tennessee

Reliability Analysis of Microturbine Components
S. F. Duffy, E. H. Baker and J. L. Palko
Connecticut Reserve Technologies, LLC

NDE Technology Development for Microturbines
W. A. Ellingson, E. R. Koehl, A. Parikh, and J. Stainbrook
Argonne National Laboratory, Argonne, Illinois

CHARACTERIZATION OF ADVANCED CERAMICS FOR INDUSTRIAL GAS TURBINE/MICROTURBINE APPLICATIONS

Oxidation/Corrosion Characterization of Monolithic Si_3N_4 and EBCs
K. L. More and P. F. Tortorelli
Oak Ridge National Laboratory, Oak Ridge, Tennessee

Mechanical Characterization of Monolithic Silicon Nitride Si_3N_4
R. R. Wills, S. Hilton, and S. Goodrich
University of Dayton Research Institute, Dayton, Ohio

Hot Section Components in Advanced Microturbines
B. Schenk, T. Strangman, D. Newson, J. Nick, J. Wimmer, and Chien-Wei Li
Honeywell Ceramic components

Microstructural Characterization of CFCCs and Protective Coatings
K. L. More
Oak Ridge National Laboratory, Oak Ridge, Tennessee

High Speed Burner Rig Development
B. Schenk and G. Schroering
Honeywell Engines, Systems & Services

DEVELOPMENT OF MONOLITHIC CERAMICS AND HIGH-TEMPERATURE COATINGS

Kennametal's Hot-Section Materials Development
R. Yeckley
Kennametal, Inc., Latrobe, Pennsylvania

Saint-Gobain Hot Section Materials Development
R. H. Licht
Saint-Gobain Ceramics & Plastics, Inc., Northboro, Massachusetts

Environmental Protection Systems for Ceramics in Microturbines and Industrial Gas Turbine Applications, Part A: Conversion Coatings
S. D. Nunn and R. A. Lowden
Oak Ridge National Laboratory, Oak Ridge, Tennessee

Environmental Protection Systems for Ceramics in Microturbines and Industrial Gas Turbine Applications, Part B: Slurry Coatings and Surface Alloying
B. L. Armstrong, K. M. Cooley, M. P. Brady, H-T Lin, and J. A. Haynes
Oak Ridge National Laboratory, Oak Ridge, Tennessee

Failure Mechanisms in Coatings
J. P. Singh, Kedar Sharma, and P. S. Shankar
Argonne National Laboratory, Argonne, Illinois

High-Temperature Diffusion Barriers for Ni-Base Superalloys
B. A. Pint, J. A. Haynes, K. L. More, and I. G. Wright
Oak Ridge National Laboratory, Oak Ridge, Tennessee

POWER ELECTRONICS

Development of High-Efficiency Carbon Foam Heat Sinks for Microturbine Power Electronics

R. D. Ott, B. L. Armstrong, J. W. Klett
Oak Ridge National Laboratory, Oak Ridge, Tennessee

Heat Exchange Concepts Utilizing Porous Carbon Foam

B. E. Thompson and A. G. Straatman
University of Western Ontario, London, Ontario, Canada

MATERIALS FOR ADVANCED RECIPROCATING ENGINES

Advanced Materials for Exhaust Components of Reciprocating Engines

P. J. Maziasz
Oak Ridge National Laboratory, Oak Ridge, Tennessee

Development of Catalytically Selective Electrodes for NOx and Ammonia Sensors

T. R. Armstrong
Oak Ridge National Laboratory, Oak Ridge, Tennessee

RECUPERATORS

Advanced Alloys for High-Temperature Recuperators

P. J. Maziasz, B.A. Pint, R. W. Swindeman, K. L. More,
J. P. Shingledecker, and N. D. Evans
Metals and Ceramics Division
Oak Ridge National Laboratory
P.O. Box 2008, Oak Ridge, TN 37831-6115
Phone: (865) 574-5082, E-mail: maziaszpj@ornl.gov

Objective

The main objective of this program is to work with commercial materials suppliers (foil and thin sheet) and recuperator manufacturers to enable manufacture and evaluation of upgraded recuperators from cost effective alloys with improved performance and temperature capability. The near term goal is better performance to or above 704°C (1300°F), and the longer-term goal is reliable performance at 760°C (1400°F) and higher.

Highlights

Materials for use to about 704°C (1300°F)

The joint project between ORNL and Allegheny-Ludlum Technical Center initiated early this year to improve the creep-resistance of commercial sheets and foils of standard 347 stainless steel at 700-750°C by modifying process has been completed. Creep testing at 704°C and 22 ksi indicates improvements of 75% for the 3.2 mil foil and 35% in rupture life for 10 mil sheet with the modified processing, now termed AL347HP. Similar creep testing of 4 and 5 mil foils of AL347HP showed even more dramatic increases of 8 and 11-14.5 times, respectively, relative to T347. Creep testing of 3.2 and 5 mil foils and 10 mil sheet of AL347HP at 750°C and 14.5 ksi showed improvements ranging from 30% to 11 times longer rupture life, particular in the 5 mil foil. Products were supplied to Ingersoll Rand Energy Systems and to Capstone Turbines. Oxidation/corrosion testing at 650°C in 10% water vapor, however, indicates very severe attack after only a few thousand hours, in several different heats of 347 steel, indicating that alloys with significantly better behavior are needed at 650-700°C.

Materials for use at 760°C (1400°F) or higher

Commercial 3.5 mil foil of HR120 from Elgiloy Specialty Metals (Elgin, IL) creep-tested at 750°C/100 MPa, lasted for 3300 h at 750°C, and is about 13 times better than standard T347 steel foil. Alloy NF709 (20Cr/25Ni, Nb, N) as about 50% longer rupture life than HR120 with a slightly lower creep rate, and alloy 625 has about 20% long life with a much lower creep rate. Commercial sheet of alloy 625 has been received from Ingersoll Rand Energy Systems for creep testing this quarter.

Technical Progress

Recuperator Component Analysis

Several different microturbine OEMs have provided pieces of fresh and engine-tested PFR and PSR recuperators made from standard 347 stainless steel for analysis, testing, and characterization. This initial baseline effort has been completed. Recuperator air cells are

manufactured from such coils of standard T347 steel, ranging from 3-4 mil foil to up to 10 mil sheet. Different kinds of recuperators include the additional manufacturing steps of welding and/or brazing. ORNL has characterized engine-tested components in order to measure the changes relative to fresh (as-manufactured) components. Detailed component analysis have been reported to each OEM. Collaborative efforts between ORNL and the various recuperator makers to incorporate materials with upgraded performance (ie., AL347HP, HR120 or alloy 625) are in progress.

Selection and Commercial Scale-Up of Advanced Recuperator Materials:
a) Materials for use to about 704°C (1300°F)

ORNL previously creep tested various standard commercial 347 steel foil and sheet at 700-750°C to establish the baseline behavior for current recuperators.

ORNL initiated a joint project with Allegheny-Ludlum Technical Center (ALTC) earlier this year to modify commercial-scale processing to improve the creep-resistance of sheet and foils of standard T347 stainless steel at 700-750°C. The objective was to provide commercial materials that Ingersoll Rand and other recuperator manufacturers could then use to produce recuperator components with improved creep-resistance at about 700°C or slightly above. Earlier, commercial 3.2 mil foil and 10 mil sheet of T347CR (now designated AL347HP) steel were creep tested at 704°C and 22 ksi, and found to have improvements of 75% for the foil and 35% compared to T347. Those products were shipped to Ingersoll Rand last quarter. Similar creep testing of 4 and 5 mil foils of the new T347CR showed even more dramatic improvements of 8 – 14.5 times better creep resistance relative to standard T347 steel. Creep testing of foils and sheet of AL347HP at 750°C and 100 MPa (14.5 ksi) also showed improvements in rupture life from 30% up to 11 time greater than standard T347, particularly the 4 and 5 mil foils (Fig. 1).

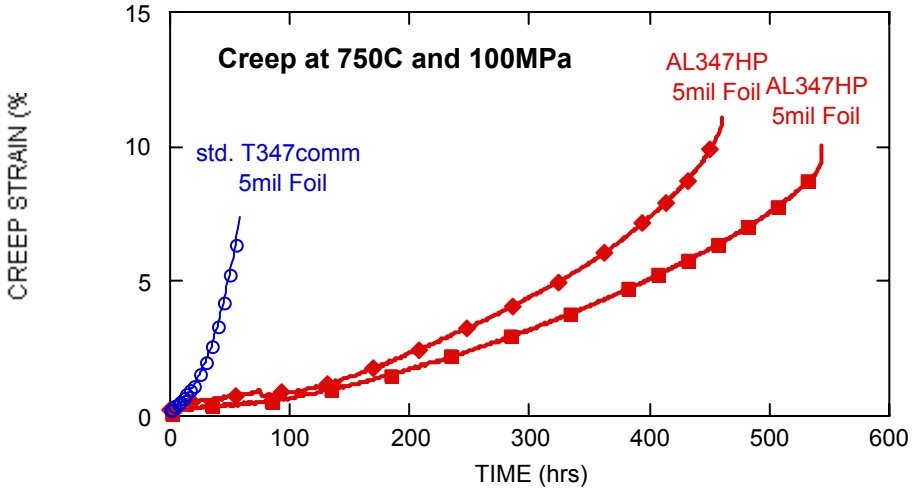

Figure 1 – ORNL creep rupture testing of standard 347 steel foils (5 mils) at 750°C and 100 MPa (14.5 ksi), comparing standard (T347) and modified (AL347HP) commercial processing conditions. This is a joint project with ORNL and Allegheny-Ludlum Technical Center.

Oxidation testing of some of the commercial foils of T347 and AL347HP steels at 650-700°C began last quarter, to compare with the large data base on the effects of water vapor enhanced oxidation at ORNL for lab-scale compositionally-modified 347 steels. Despite improvements in creep-resistance, the commercial foils behaved similar to other heats of 347 steel, with rapid breakaway after several thousand hours even at this lower temperature (Fig. 2).

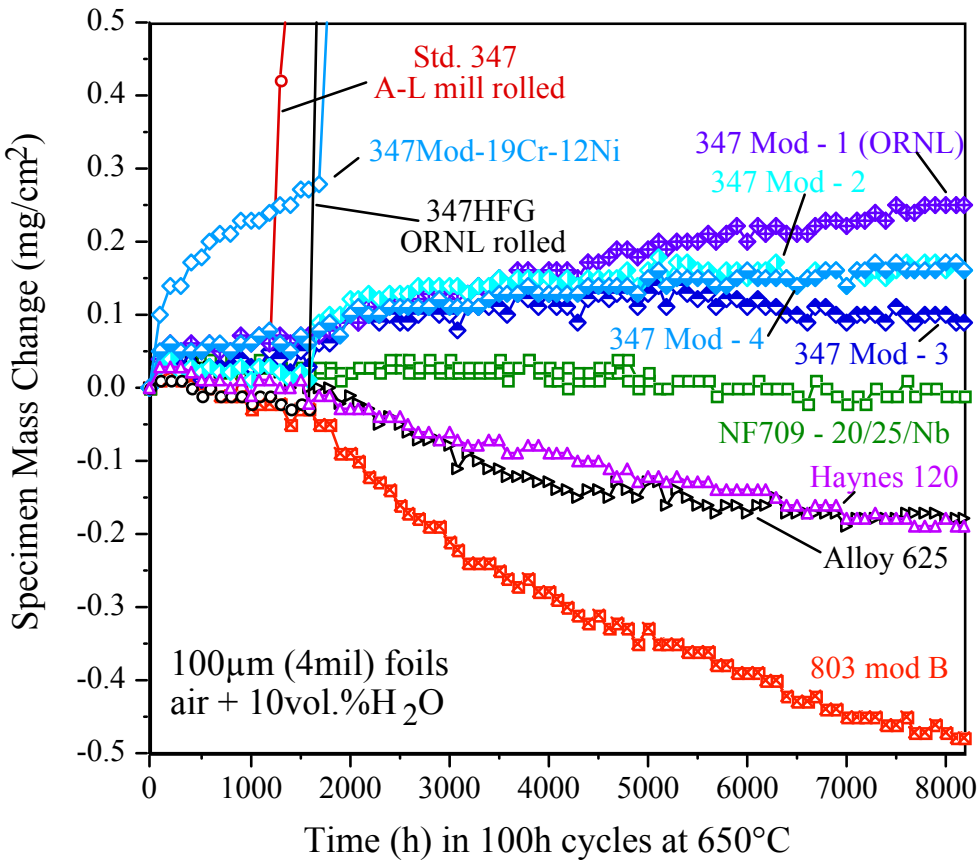

Figure 2 – ORNL oxidation test data for coupons of foils of various commercial and developmental stainless steels, stainless alloys or nickel-based superalloys, processed at ORNL or commercially and tested at 650°C in 10% water vapor. Specimens are cycled every 100h to be weighed. Note the rapid breakaway oxidation of several foils of standard 347 steel composition. Standard 347, A-L mill rolled is the 5 mil T347 steel foil from the joint ORNL/ALTC project.

<u>b) Materials for use at 760°C (1400°F) or higher</u>

HR 120 (Fe-25Cr-35Ni) is one of the more promising commercially available material with significantly better creep-resistance and corrosion-resistance in this temperature range at 3-4 times the cost of 347 stainless steel. Commercial 3.5 mil foil of HR120 was obtained by ORNL from Elgiloy Specialty Metals (Elgin, IL) and creep-tested at 704°C/152 MPa, and at 750°C/100 MPa. The HR 120 foil lasted 900h at 704°C, and lasted for 3300 h at 750°C, both with good rupture ductility. The creep resistance of HR 120 at 750°C is about 13 times better than standard 347 steel foil with standard commercial processing (Fig. 3). Creep data is also included for NF709 (Fe-20Cr-25Ni, Nb,N), from boiler tubing that was split and rolled into foil at ORNL. The NF709 shows about 50% longer rupture life than HR120. Alloys 625 and HR214 show roughly similar creep rupture resistance, but have much lower creep rates.

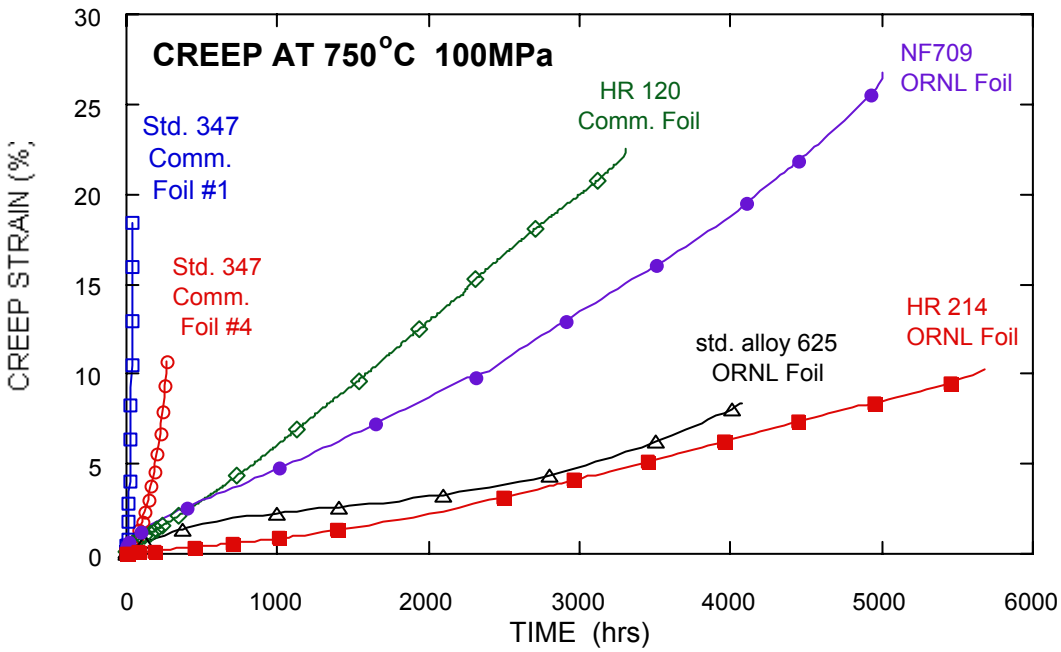

Figure 3 – Comparison of creep rupture curves for testing of commercial or ORNL processing of 4 mil foils of high performance alloys at 750°C and 100 MPa (14.5 ksi). Foils include commercial HR120, and ORNL processed foils of NF709, alloy 625 and HR 214.

The commercial HR 120 foil and ORNL foils of alloy 625 and NF709 have also been incorporated into the oxidation testing matrix, and at 650-750°C are resistance to water-vapor enhanced oxidation, at least to about 8000 h (Fig. 2). Oxidation testing will continue next quarter, and many of these steels and alloys will also be incorporated into the ORNL Recuperator testing facility next quarter.

Status of Milestones

FY2003 – Produce standard 347 steel with modified commercial processing to maximize creep resistance for sheet and foil gages. Certify properties and provide sufficient creep-resistant 347 steel to microturbine OEMs to manufacture recuperators with improved performance for use at or slightly above 700°C (April 2003). (Completed)

Industry Interactions

Microturbine OEM Ingersoll-Rand Energy Systems took delivery of the new AL347HP sheet and foils processed by Allegheny-Ludlum and ORNL for improved creep resistance for recuperator manufacturing. Capstone Turbines also took delivery of some 5 mil foil of the AL347HP for testing and evaluation. Ingersoll Rand sent ORNL pieces of several engine tested and fresh recuperators (mainly 347 steel, but also some alloy 625) for microcharacterization analysis and evaluation. ORNL and Ingersoll Rand have also begun braze alloy studies in support of their advanced recuperator manufacturing efforts

Problems Encountered

None

Publications/Presentations

P. J. Maziasz, R. W. Swindeman, J. P. Shingledecker, K. L. More, P. A. Bint, E. Lara-Curzio, and N. D. Evans, "Improving High-Temperature Performance of Austenitic Stainless Steels for Advanced Microturbine Recuperators," paper was presented at the 6th International Charles Parsons Turbine Conference, held September 16-18, 2003 in Dublin, Ireland; paper is pp. 1057-1073 of Parsons 2003: Engineering Issues in Turbine Machinery, Power Plants and Renewables, Institute for Materials, Minerals and Mining, Maney Publishing, London, UK (2003).

Recuperator Alloys – Composition Optimization for Corrosion Resistance

B. A. Pint
Metals and Ceramics Division
Oak Ridge National Laboratory
Oak Ridge, TN 37831-6156
Phone: (865) 576-2897, E-mail: pintba@ornl.gov

Objective

In order to provide a clear, fundamental understanding of alloy composition effects on corrosion resistance of stainless steel components used in recuperators, the oxidation behavior of model alloys is being studied. The first phase of this study narrowed the range of Cr and Ni contents required to minimize the accelerated corrosion attack caused by water vapor at 650°-800°C. Other factors that continue to be investigated include the effects of temperature, alloy grain size, phase composition and minor alloy additions. These composition and microstructure effects also will provide data for life-prediction models and may suggest a mechanistic explanation for the effect of water vapor on the oxidation of steels. This information will be used to select cost-effective alloys for higher temperature recuperators.

Highlights

The oxidation behavior of model austenitic alloys is being studied in order to better understand the role of minor alloy additions on the accelerated attack (AA) observed in exhaust gas at 650°C-700°C. Results from a series of alloys based on Fe-(16-20)Cr and (15-20)Ni illustrated that the leaner compositions Fe-16Cr-15Ni all were susceptible to AA in humid air at 650°C despite various additions of Mn, Si and/or La. When the Cr and/or Ni content was increased to 20% in the base alloy, additions of Mn and Si significantly improved resistance to AA. For a base alloy of Fe-20Cr-20Ni, single additions of Mn, Si and La did not prevent the onset of AA. However, when both Mn and Si were added, no AA has been observed after more than 5,000h of testing at 650°C in humid air.

Technical Progress

Experimental Procedure

As outlined in previous reports, model alloys were vacuum induction melted and cast in a water-chilled copper mold, followed by hot forging and rolling to 2.5mm. The sheets were then cold rolled to 1.25mm and annealed under Ar + 4%H_2 for 2 min at 1000°C. Sheet specimens (12mm x 17mm x 1.2mm) were polished to 600 grit SiC finish. Chemical compositions were measured by combustion and plasma analysis after casting, Table I. The oxidation tests were done in air + 10vol.% water vapor with 100h cycles at 650°. After oxidation, selected specimens were Cu-plated, sectioned and polished to examine the oxide scale.

Results of oxidation testing

Previous work on model ferritic alloys had shown that Mn and Si were two of the most beneficial minor alloy additions for preventing AA and retaining a thin, protective surface oxide. (High mass gains after the onset of AA indicate the formation of a thick oxide, while large mass losses indicate

Table 1. Alloy chemical compositions (mass %) and average grain sizes (μm)

Material	Cr	Ni	Mn	Si	C	N	Nb	Ti	Mo	Other	aver. grain size
Fe-20Cr-20Ni	19.7	20.1	<	0.01	<	<	<	<	<		14μm
Fe-16Cr-15Ni	15.8	14.8	<	<	0.002	<	<	<	<		24
Fe-16Cr-15Ni+Mn	16.0	15.0	1.66	0.01	0.002	0.001	<	<	<		≈15
Fe-16Cr-15Ni+Si	16.2	14.7	<	0.17	<	0.001	<	<	<		
Fe-16Cr-15Ni+La	16.1	14.9	<	0.01	0.001	0.02	<	<	<	0.17 La	
Fe-16Cr-15Ni+MS	15.8	14.8	1.76	0.24	<	<	<	<	<		
Fe-16Cr-15Ni+MSL	17.0	14.1	1.74	0.24	0.002	0.001	<	<	<	0.17 La	
Fe-16Cr-20Ni+MS	15.8	19.7	1.72	0.24	0.003	0.001	<	<	<		
Fe-20Cr-15Ni+MS	19.8	14.9	1.70	0.24	0.001	0.007	<	<	<		
Fe-20Cr-20Ni+Mn	20.0	19.8	1.47	0.01	0.002	0.001	<	<	0.01		
Fe-20Cr-20Ni+Si	19.9	19.7	<	0.23	0.001	0.005	<	<	<		
Fe-20Cr-20Ni+La	20.3	19.7	<	<	0.001	0.001	<	<	<	0.10 La	
Fe-20Cr-20Ni+MS	19.8	19.8	1.69	0.25	<	0.003	<	<	<		
Fe-20Cr-20Ni+MSL	20.2	19.9	1.61	0.22	0.001	0.011	<	<	<	0.12 La	
Fe-20Cr-20Ni+etc.	20.9	20.8	3.8	0.24	0.08	0.18	0.25	<	0.31	0.3 Cu, 0.3Co	

< indicates below the detectability limit of <0.01% or <0.001% for interstitials

the spallation of the thick oxide.) In order to clarify the role of these additions in austenitic alloys, model alloys were made with various additions of Mn, Si and La, Table I. Figure 1a shows the 650°C performance of various alloys with a base composition of Fe-16Cr-15Ni. All of the additions showed

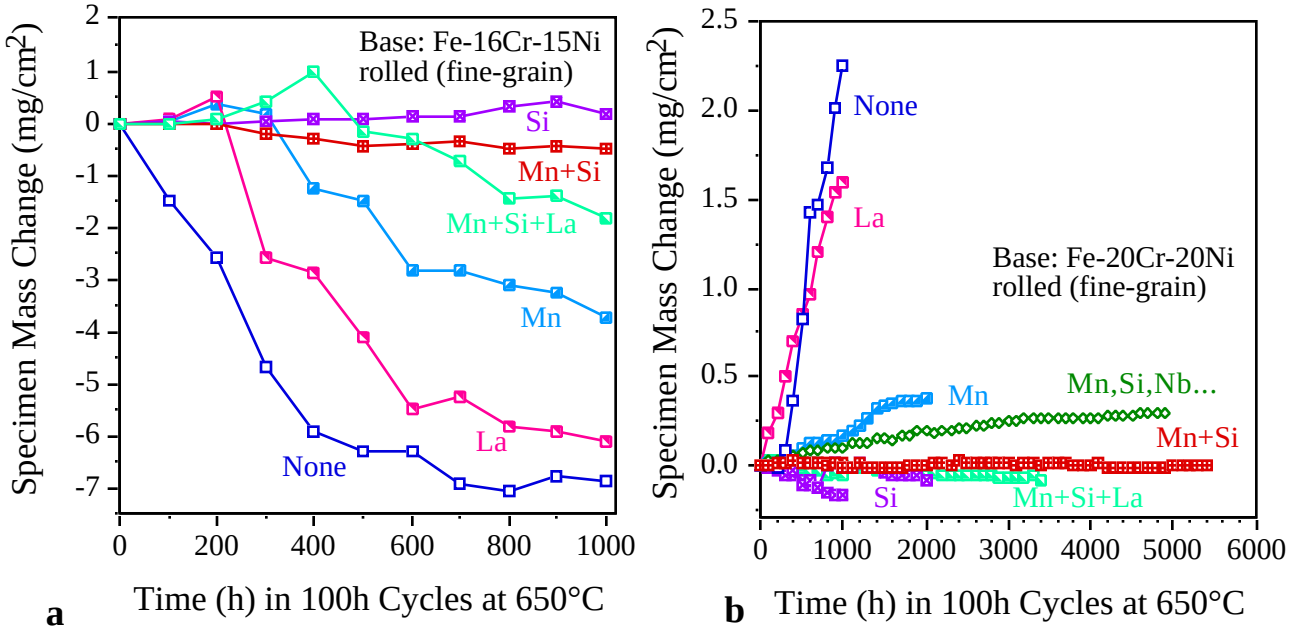

Figure 1. Specimen mass changes for model Fe-Cr-Ni alloys during 100h cycles at 650°C in air plus 10%H_2O, (a) alloys with a base composition of Fe-16Cr-15Ni and (b) alloys with a base composition of Fe-20Cr-20Ni. Note the change in the y-axis range between (a) and (b).

less mass loss than the base alloy without additions, but all of the modified alloys showed AA to some degree. Single additions of La or Mn showed the least benefit. Surprisingly, the addition of Si alone showed less mass change than the additions with Si in combination with Mn or Mn and La. In general, these results suggest that the base Fe-16Cr-15Ni alloy is too lean in Cr and Ni to be protective under these conditions. With a base composition of Fe-17Cr-11Ni, a similar inference can be drawn about type 347 stainless steel.

Figure 1b shows the performance of various modifications of a base Fe-20Cr-20Ni alloy at 650°C. Again, single additions of Mn or La did not show a significant beneficial effect. The onset of AA was slowed by the Mn addition but not prevented. Linear mass losses were observed for the alloy with only a Si addition. These small mass losses are attributed to evaporation of Cr from the scale. However, the edges of the specimen showed evidence of the onset of AA. The addition of both Mn and Si led to a low mass change past 5,000h thus demonstrating a synergistic benefit of adding both elements. Adding La in addition to Mn and Si has not shown any additional benefit at this stage of the testing, Figure 1b. The first attempt to develop a creep-resistant version of Fe-20Cr-20Ni contains additions of Mn, Si, Nb and several other elements, Table I. The oxidation behavior of this material also is shown in Figure 1b. The mass gain is higher than the model alloy with only Mn and Si additions but no AA has been observed after almost 5,000h. The higher mass gain is attributed to its higher Mn content which can lead to additional Mn-rich spinel formation.

Since the best long-term behavior was noted with additions of Mn and Si, additional model alloys were made with different Cr and Ni contents. Figure 2 shows the performance of several of these alloys at 650°C in humid air compared to the base model alloys without Mn and Si additions. In each case, the addition of Mn and Si improved the resistance to AA compared to the base alloy. However, as noted above, with Fe-16Cr-15Ni, the addition of Mn and Si reduced the mass loss compared to the

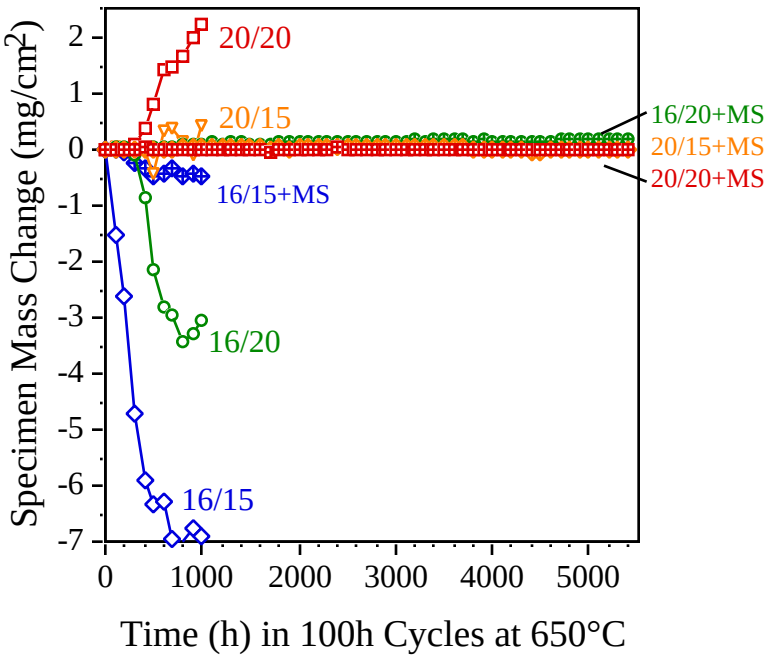

Figure 2. Specimen mass changes for model Fe-Cr-Ni alloys (specified by their Cr/Ni contents) during 100h cycles at 650°C in air plus 10%H_2O. Designations with "+MS" indicate Mn and Si additions.

base alloy but did not prevent AA. Figure 3a shows the scale cross-section after 1000h at 650°C on Fe-16Cr-15Ni+Mn,Si. The typical duplex scale was observed with an outer Fe-rich oxide and an inner mixed Fe, Cr, and Ni oxide. A similar oxide was observed on all of the model alloys without Mn and Si additions. For example, Figure 3b shows the scale formed on Fe-20Cr-20Ni after 1000h. Increasing either the Cr or Ni content to 20% and adding Mn and Si eliminated the onset of AA to over 5,000h, Figure 2. Cross-sections of Fe-16Cr-20Ni+Mn,Si and Fe-20Cr-15Ni+Mn,Si after 1,000h at 650°C are shown in Figures 3c and 3d, respectively. A few oxide nodules were observed on the former material but based on the low, long-term mass gain, the nodules did not continue to grow significantly. Only small nodules were observed on Fe-20Cr-15Ni+Mn,Si, Figure 3d. Increasing the Cr and Ni contents to 20% with the additions of Mn and Si resulted in very little mass change after a 5,000h exposure at 650°C and a uniform thin scale, Figure 3e. Because of its thin scale and low mass change, this alloy is considered the most promising composition for further development.

Some of the other model alloys also were sectioned and are shown in Figure 3. The mass losses noted for Fe-20Cr-20Ni+Si resulted in a thin scale after a 1000h exposure at 650°C, Figure 3f. The higher mass gain for Fe-20Cr-20Ni+Mn can be attributed to the large oxide nodules observed in Figure 3g.

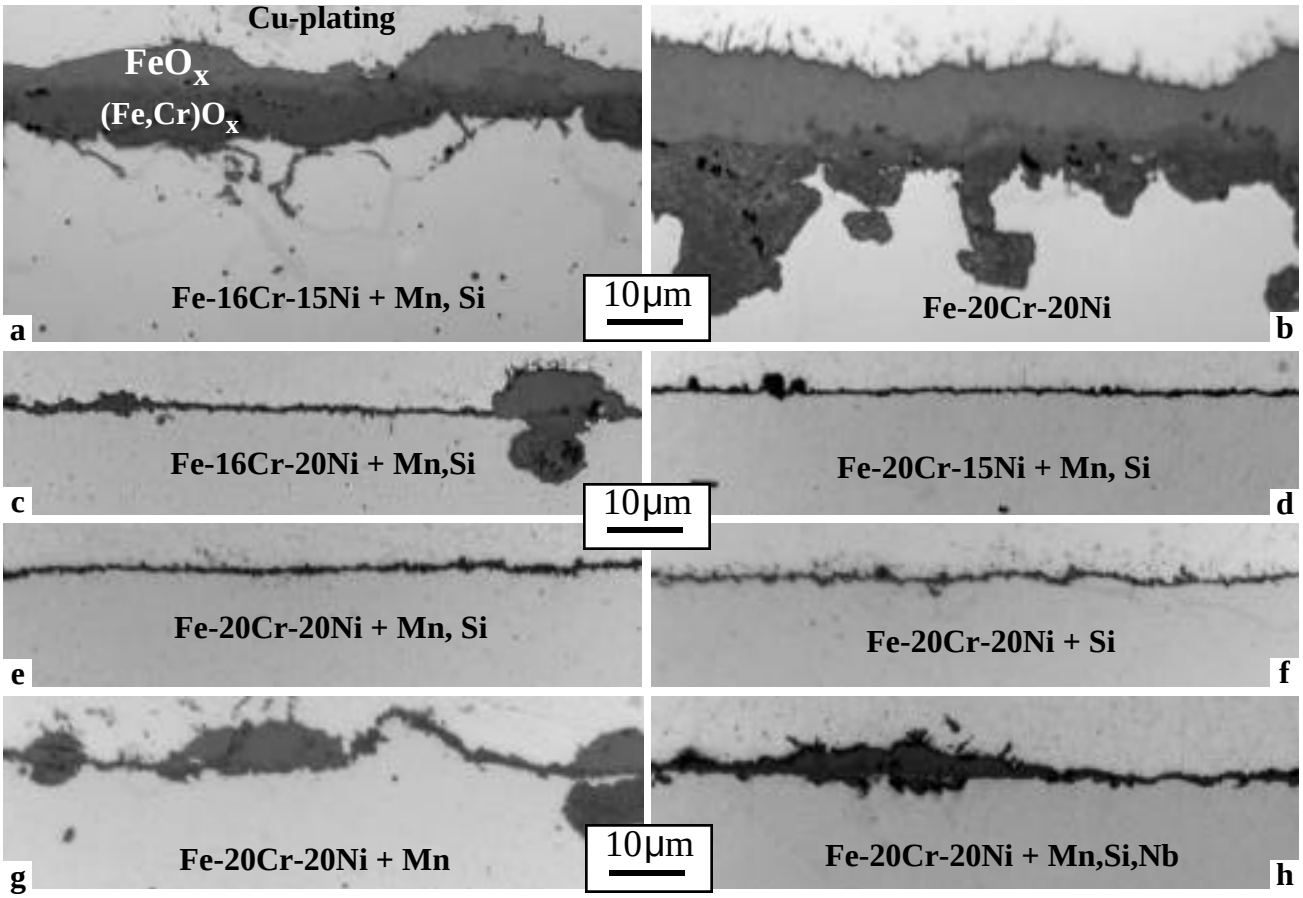

Figure 3. Light microscopy of polished cross-sections of model alloys oxidized for 1000h at 650°C in humid air (a) Fe-16Cr-15Ni+Mn,Si, (b) Fe-20Cr-20Ni, (c) Fe-16Cr-20Ni+Mn,Si, (d) Fe-20Cr-15Ni+Mn,Si, (e) Fe-20Cr-20Ni+Mn,Si, (f) Fe-20Cr-20Ni+Si, (g) Fe-20Cr-20Ni+Mn, and (h) Fe-20Cr-20Ni+Mn,Si,etc.

Finally, Figure 3h shows the thicker scale formed on the creep-resistant version of Fe-20Cr-20Ni, likely due to its higher level of alloy additions. Future development work will examine alloy additions that improve the alloy creep strength while minimizing the scale thickness.

Status of Milestones

Draft a report summarizing results on the use of minor alloy additions to improve corrosion performance in exhaust gas environments. (January 2003) Completed - NACE Paper #03-499.

Industry Interactions

Visited Ingersoll Rand in New Hampshire in July 2003 to discuss materials selection issues.

Provided oxidation data on alloy foils to Wendy Matthews at Capstone.

Problems Encountered

None.

Publications/Presentations

None.

Recuperator Materials Testing and Evaluation

Edgar Lara-Curzio, Rosa Trejo and K. L. More
Metals and Ceramics Division
Oak Ridge National Laboratory
P.O. Box 2008, Oak Ridge, TN 37831-6069
Phone: (865) 574-1749, E-mail: laracurzioe@ornl.gov

Objective

The objective of this sub-task is to screen and evaluate candidate materials for the next generation of advanced microturbine recuperators. To attain this objective, a commercially-available microturbine was acquired and in coordination and collaboration with its manufacturer, it was modified to operate at recuperator inlet temperatures as high as 843°C. The durability of candidate recuperator materials will be determined by placing test specimens at a location upstream of the recuperator, followed by determination of the evolution of the material's physical and mechanical properties as a function of time of exposure. During exposure tests inside the microturbine, it will be possible to subject test specimens to various levels of mechanical stress by using a specially-designed sample holder and pressurized air. The selection of materials to be evaluated in the modified microturbine will be made in coordination and collaboration with other tasks of this program and with manufacturers of microturbines and recuperators.

Highlights

The first two 500-hr test campaigns to evaluate foils of 347 stainless steel and Haynes 230 Alloy have been completed. A test campaign is in progress to evaluate Haynes 230 and HR-120 alloys.

Technical progress

In this document we report the results from the first 500-hr test campaign during which foils of 347 stainless steel were evaluated in ORNL's recuperator testing facility.

Evaluation of baseline properties of 347 stainless steel foils.
The foil materials used in this investigation were received from Capstone Turbine Corp. in the form of a roll 20.3-cm wide and 0.089-mm thick. Miniature dog-bone shaped test specimens, with their principal axis aligned either parallel or perpendicular to the rolling direction, were obtained by electric discharge machining as illustrated in Figure 1.

The tensile behavior of the miniature test specimens was determined at ambient conditions using a procedure described in detail in a previous report[1]. The tests were carried out at a constant crosshead displacement rate and both the load and crosshead displacement were recorded during the test. Because of the small dimensions of the test

[1] E. Lara-Curzio, "Recuperator Materials Testing and Evaluation" in DER Materials Program Quarterly Report, January-March, 2003

specimens it was not possible to measure directly the tensile strain of the test specimens, but values of strain were determined from the crosshead displacement data after applying a correction for the compliance of the load train. This procedure is described in detail in Appendix A at the end of this report.

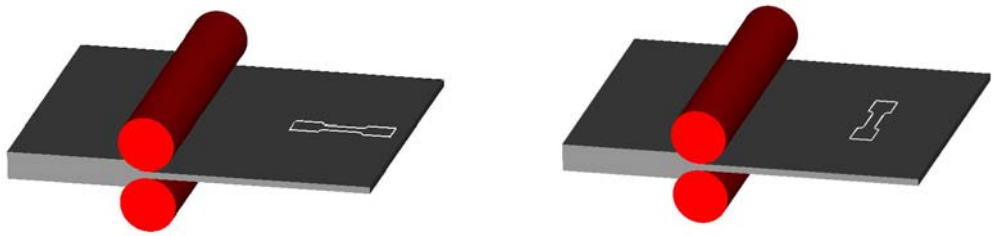

(a) (b)

Figure 1. Orientation of miniature tensile specimens (a) along and (b) perpendicular to the to rolling direction.

Figures 2 and 3 show stress versus strain curves obtained from the tensile evaluation of test specimens that had been cut either parallel or perpendicular to the foil rolling direction. The tensile stress-strain curves are characterized by: a well-defined linear region associated with elastic deformation, a well-defined transition to plastic deformation, and extensive ductility with the failure strain exceeding 70%.

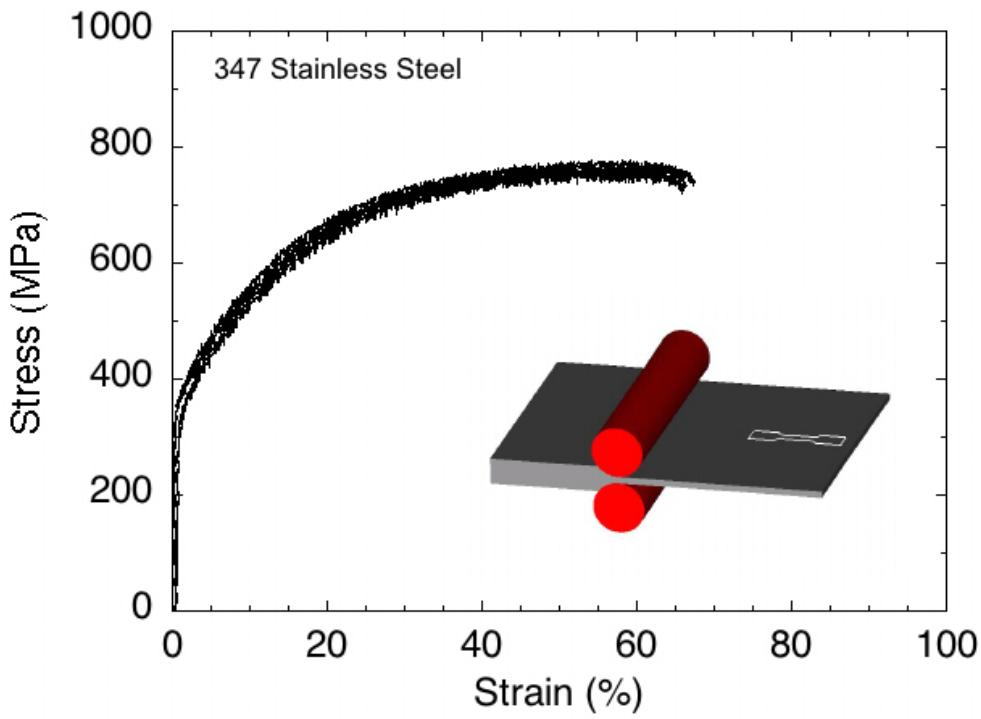

Figure 2. Stress-strain curves obtained from the tensile evaluation of miniature test specimens of 347 stainless steel 0.089-mm thick foils. Test specimens were obtained along the rolling direction.

Table I summarizes the values for the 0.2% yield strength, the ultimate tensile strength and the strain at failure. An analysis of variance showed that the differences between the tensile strength of specimens cut along the rolling direction and perpendicular to the rolling direction were significant at the 95% confidence level. These results are

consistent with the higher strength and lower ductility that are expected for materials that have been strain-hardened.

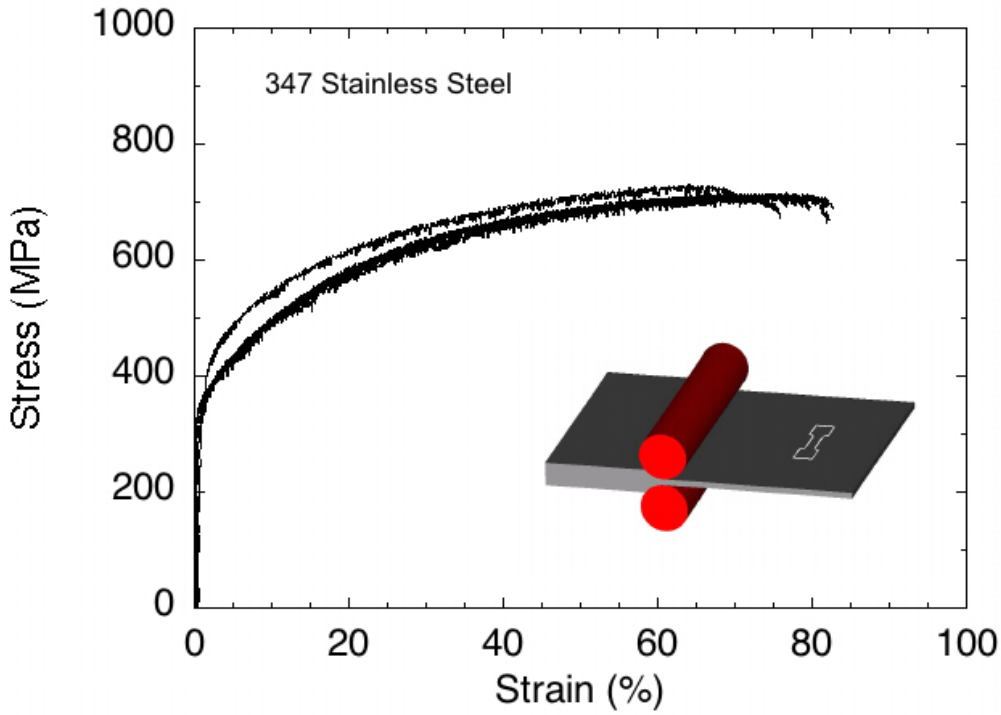

Figure 3. Stress-strain curves obtained from the tensile evaluation of miniature test specimens of 347 stainless steel 0.089-mm thick foils. Test specimens were obtained perpendicular to the rolling direction.

Table I. Summary of tensile results for as-processed materials.

347 Stainless Steel	0.2% Yield Strength (MPa)	Ultimate Tensile Strength (MPa)	Strain at Failure (%)
⊥ to rolling direction	384 ± 33	717 ± 7	78 ± 5
‖ to rolling direction	379 ± 16	766 ± 8	66 ± 1

Figure 4 contains an optical micrograph showing miniature test specimens before and after tensile testing. It can be observed that the failure plane of the tested specimen is at 45° with respect to the loading direction, which occurs when high-density slip planes become aligned parallel to this plane after the test specimen has experienced extensive deformation. Examination of the fracture surface revealed the presence of dimples, which are characteristic of ductile failure.

Evaluation of 347 stainless steel foils in ORNL's microturbine test facility.

Four 0.089-mm thick, 75-mm long and 14-mm wide 347 stainless steel foils were laser-welded onto a 347 stainless-steel sample holder as illustrated in Figure 5. The diameter of sample holder onto which the foils were welded was 23.1 mm. Prior to welding the foils, type-K thermocouples were placed in each one of the four holes in the sample holder. These holes are also used to allow the flow of air for mechanical stressing the foils through the internal pressurization of the sample holder. The sample holder was inserted into the modified C60 microturbine through one of the custom-made ports as illustrated in Figure 6 and the microturbine was operated for 500 hours with the settings listed in Table II.

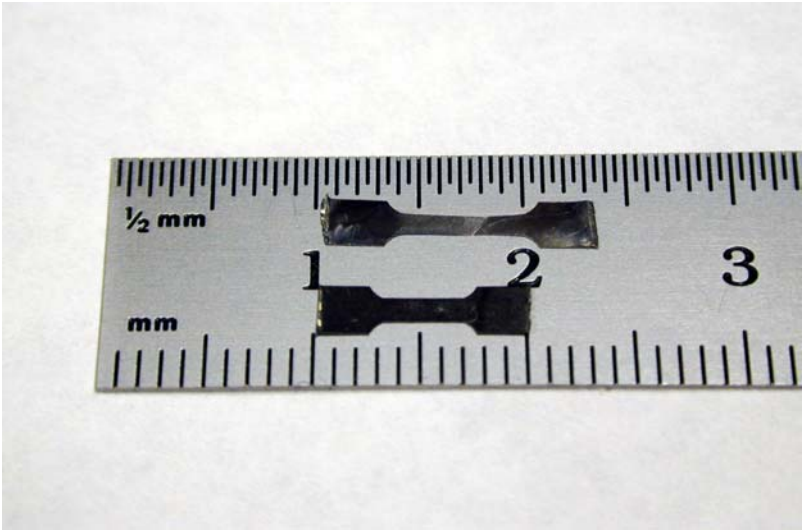

Figure 4. Optical micrograph of as-processed 347 stainless steel after tensile evaluation at ambient conditions. Note that the fracture plane is aligned at 45° with respect to the loading direction.

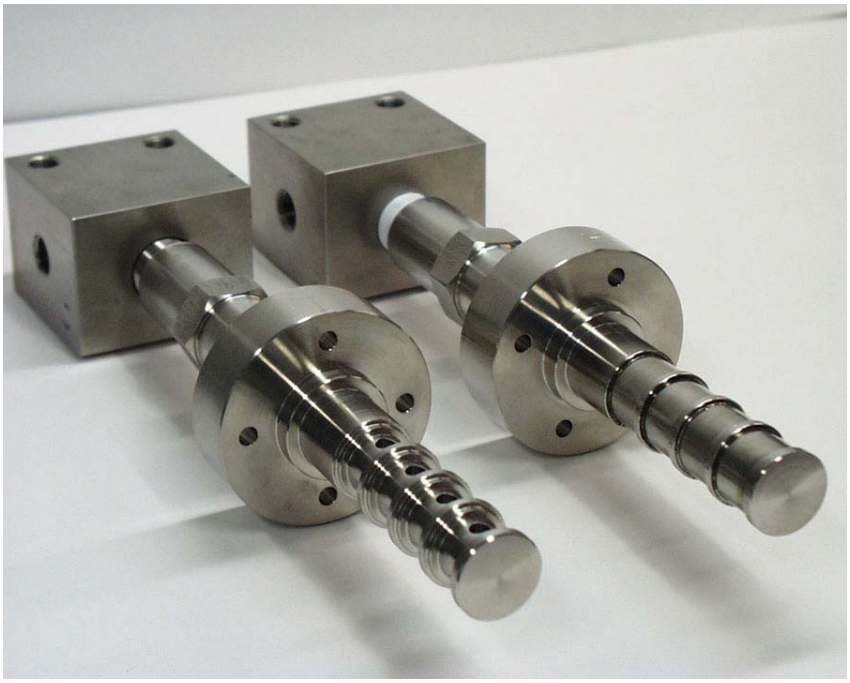

Figure 5. Sample holders with and without foils. The holes in the sample holder allow the placement of thermocouples and the flow of air for mechanically stressing the foils through the internal pressurization of the sample holder.

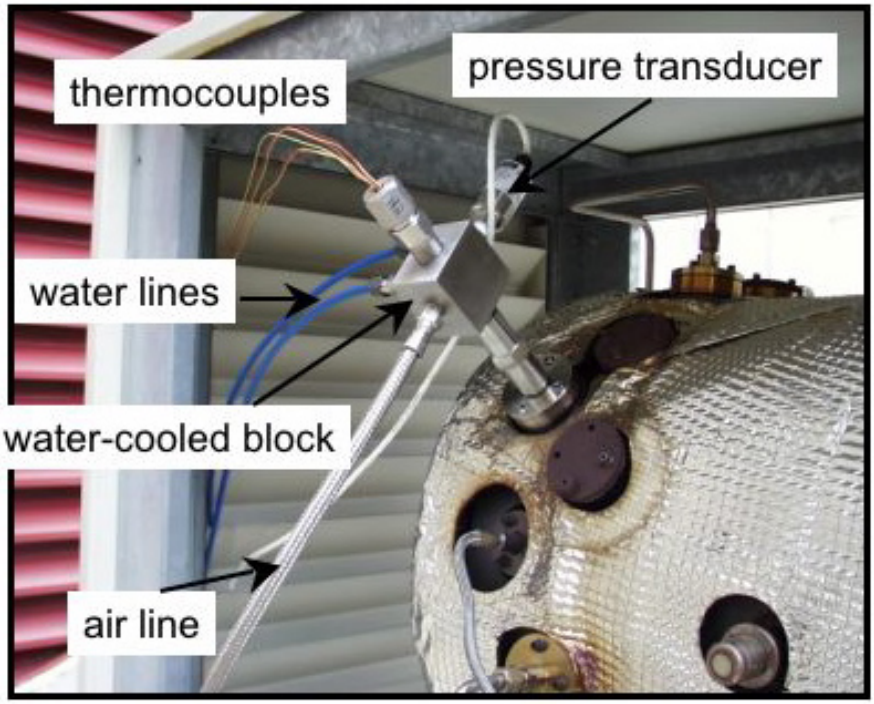

Figure 6. Photograph illustrating the placement of test specimens in ORNL's microturbine recuperator testing facility.

Table II. Microturbine settings for 500-hr test.

Engine Speed	45,000 RPM
Turbine Exit Temperature	800°C
Fuel	natural gas

After issuing the microturbine "start command" the sample holder was allowed to reach thermal equilibrium in 30 minutes. At that point, the sample holder was pressurized to 63 psi using plant air and the pressure was maintained constant for the duration of the test. This value of pressure results in a tensile tangential stress of 50 MPa on the foils. Figure 7 shows a picture of the system used to maintain constant pressure inside the sample holders. The system includes a pressure regulator, a digital pressure controller, a transducer for feedback control, a solenoid valve and a relief valve. The pressure controller was programmed to open the solenoid valve whenever the pressure dropped below 61 psi. Therefore, by having a continuous record of the value of the pressure it was possible to know when the specimen increased in volume, which would be indicative of the occurrence of creep deformation. By selecting a narrow dead band for the pressure controller, fatigue effects were avoided. In addition to the magnitude of the pressure, the temperature of the four foils and the turbine exit temperature were recorded during the test, as illustrated by the temperature history in Figure 8. Unfortunately a faulty contact prevented the recording of the temperature of foil D, but calibration information was used to determine this value. Figure 9 shows the temperature distribution along the length of the sample holder for a turbine exit temperature of 800°C. The curve in Figure 8, which was obtained using a single thermocouple that was carefully positioned inside the sample holder during microturbine operation, illustrates the beauty of this test configuration, namely the ability to obtain information on the effects of mechanical stress and exposure

to microturbine exhaust gases on the foils under evaluation over a temperature interval of almost 125°C for a TET value of 800°C.

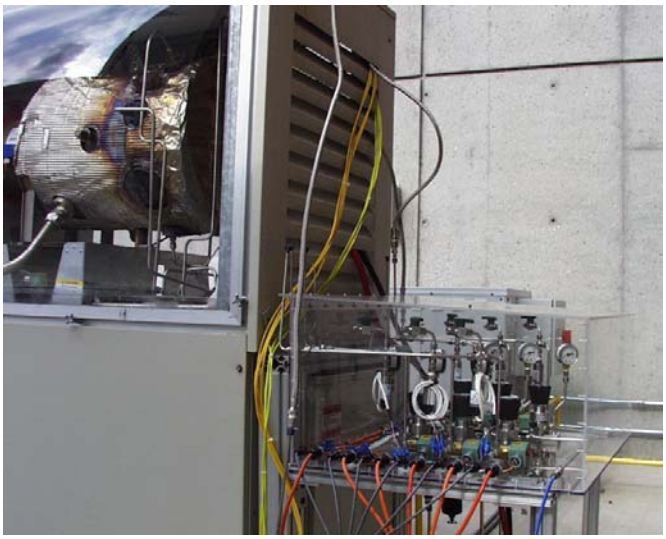

Figure 7. Set-up for pressurization of sample holders.

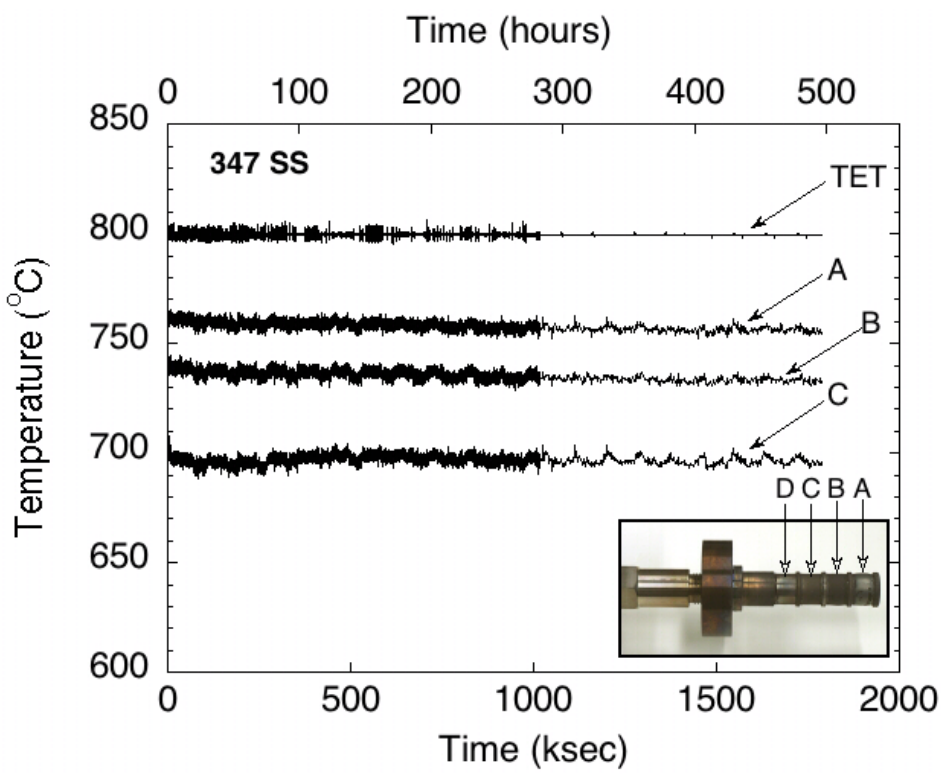

Figure 8. Temperature history for 500-hr test to evaluate the behavior of 0.089-mm thick foils of 347 stainless steel.

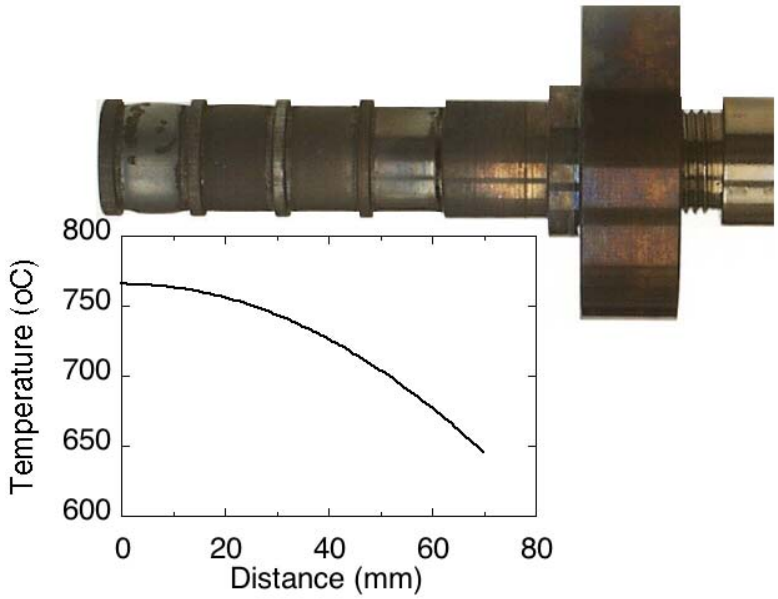

Figure 9. Temperature distribution along stainless sample holder for TET=800°C.

Post-test analysis

At the end of the 500-hr test, the sample holder was removed from the microturbine. It was necessary to handle it with extreme care because the oxide layer that had formed on foil A had partially spalled. Figures 10 to 15 are optical micrographs of the sample holder and foils taken shortly after they were removed from the microturbine. It was evident, as illustrated in Figure 10, that foil A had "ballooned" as a result of creep deformation. After photographic documentation the foils were removed from the sample holder using a lathe and a diamond tool. Longitudinal segments from each foil specimen were cut for microstructural characterization, while miniature tensile specimens were obtained by electric discharge machining from the remaining material (Figures 16-17).

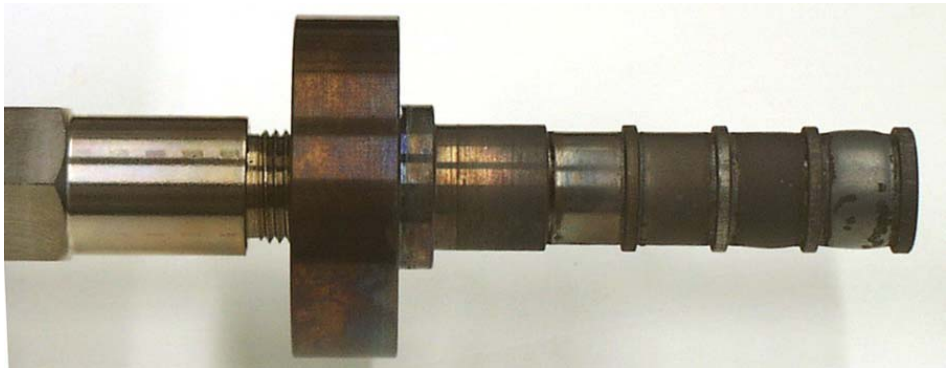

Figure 10. Optical micrograph of sample holder with of 0.089-mm thick foils of 347 stainless steel after 500-hr test at TET=800°C and tensile tangential stress of 50 MPa. Note the ballooning of foil A due to creep deformation and the scale on the surface of the foils.

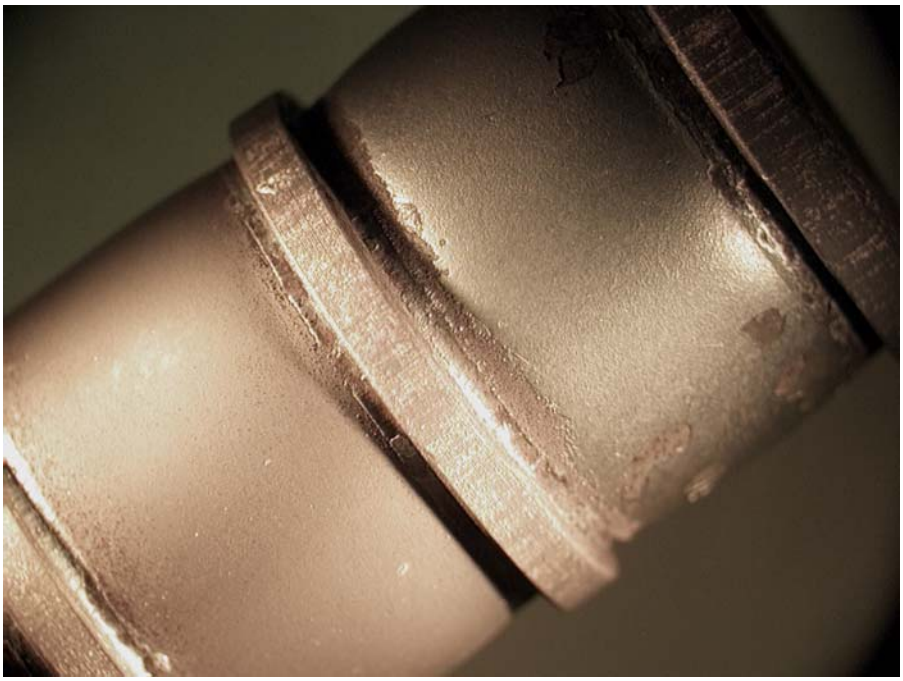

Figure 11. Optical micrograph of foils A and B (0.089-mm thick foils of 347 stainless steel), after 500-hr test at a TET of 800°C and tensile tangential stress of 50 MPa.

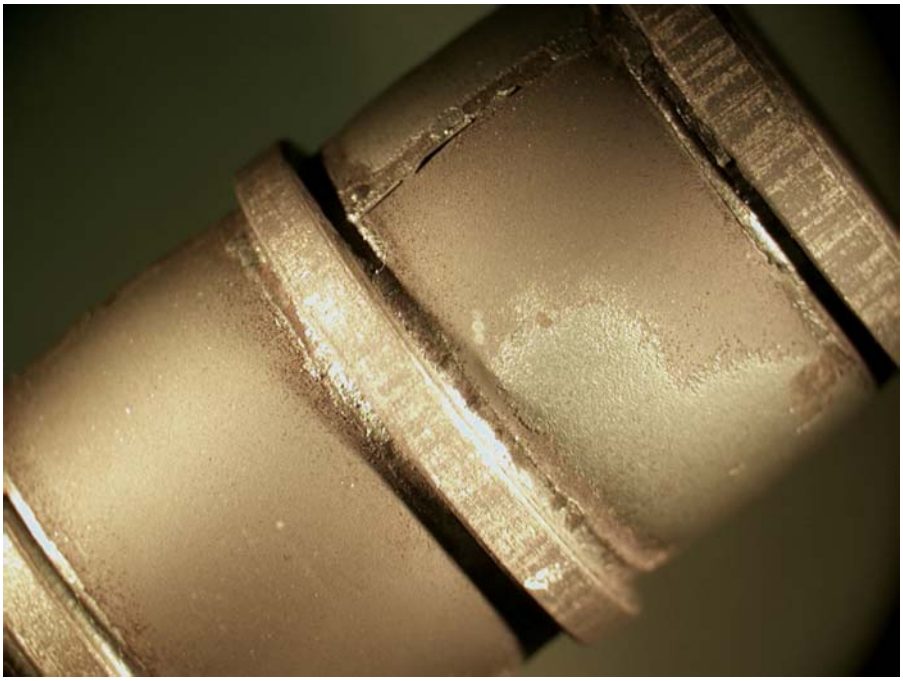

Figure 12. Optical micrograph of foils A and B (0.089-mm thick foils of 347 stainless steel), after 500-hr test at a TET of 800°C and tensile tangential stress of 50 MPa. Note the corrosion scale on the surface of the foils. The weld seam in foil A is evident.

Figure 13. Optical micrograph of foils A and B (0.089-mm thick foils of 347 stainless steel), after 500-hr test at a TET of 800°C and tensile tangential stress of 50 MPa. Note the corrosion scale on the surface of the foils. The weld seam in foil B is evident.

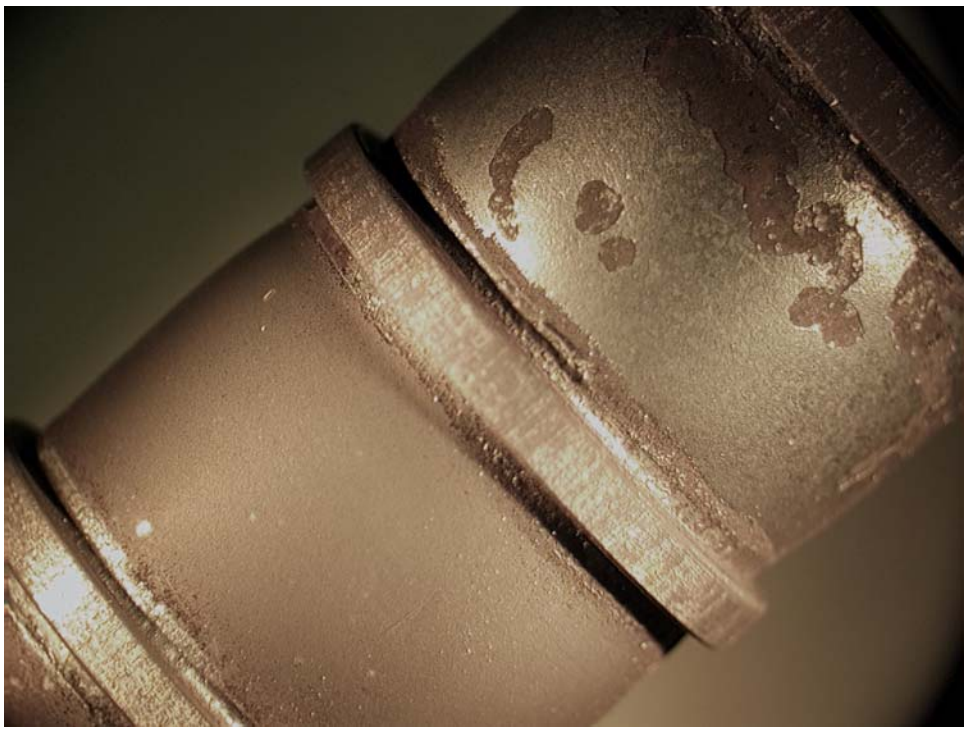

Figure 14. Optical micrograph of foils A and B (0.089-mm thick foils of 347 stainless steel), after 500-hr test at a TET of 800°C and tensile tangential stress of 50 MPa. Note the corrosion scale on the surface of the foils.

Figure 15. Optical micrograph of foils C and D (0.089-mm thick foils of 347 stainless steel), after 500-hr test at a TET of 800°C and tensile tangential stress of 50 MPa. Note the laser-weld seam.

Figure 16. Stainless steel specimen after removal from sample holder.

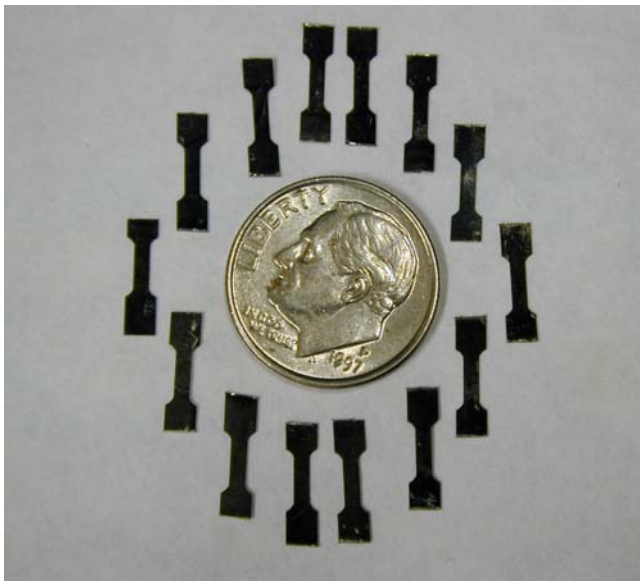

Figure 17. Miniature stainless steel tensile specimen obtained by electric discharge machining from foil specimen.

A total of 14 miniature tensile specimens were obtained from each foil, except from foil A, which had been exposed to the highest temperatures and from which only 6 useful tensile specimens were obtained. It was found that foil A was severely damaged and had several longitudinal cracks, as illustrated by the scanning electron micrograph in Figure 18. The miniature tensile specimens were evaluated under the same conditions used to evaluate the as-processed foils.

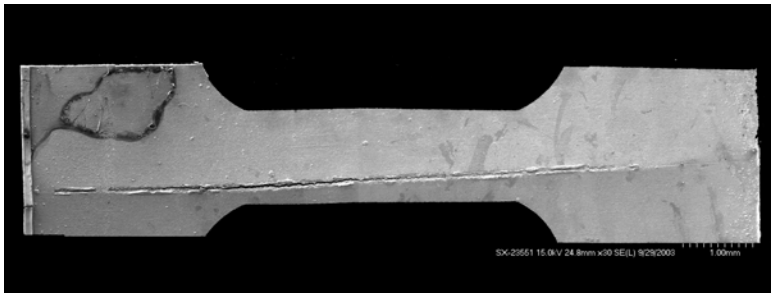

Figure 18. Scanning electron micrograph of miniature tensile specimen obtained from A (0.089-mm thick foil of 347 stainless steel) after 500-hr test. Note the longitudinal crack.

Figures 19 to 22 contain stress versus strain plots obtained from the evaluation of miniature 347 stainless steel tensile specimens after 500-hr exposure in the ORNL microturbine recuperator testing facility. The stress-strain curves in Figure 19, which correspond to test specimens obtained from foil A, reveal a significant decrease in both the tensile strength and ductility of the material as a result of exposure to mechanical stress and microturbine environment. While the ultimate tensile strength of foils B, C and D was lower than that of the as-processed material, the most significant changes occurred on the residual ductility. Table III summarizes these results.

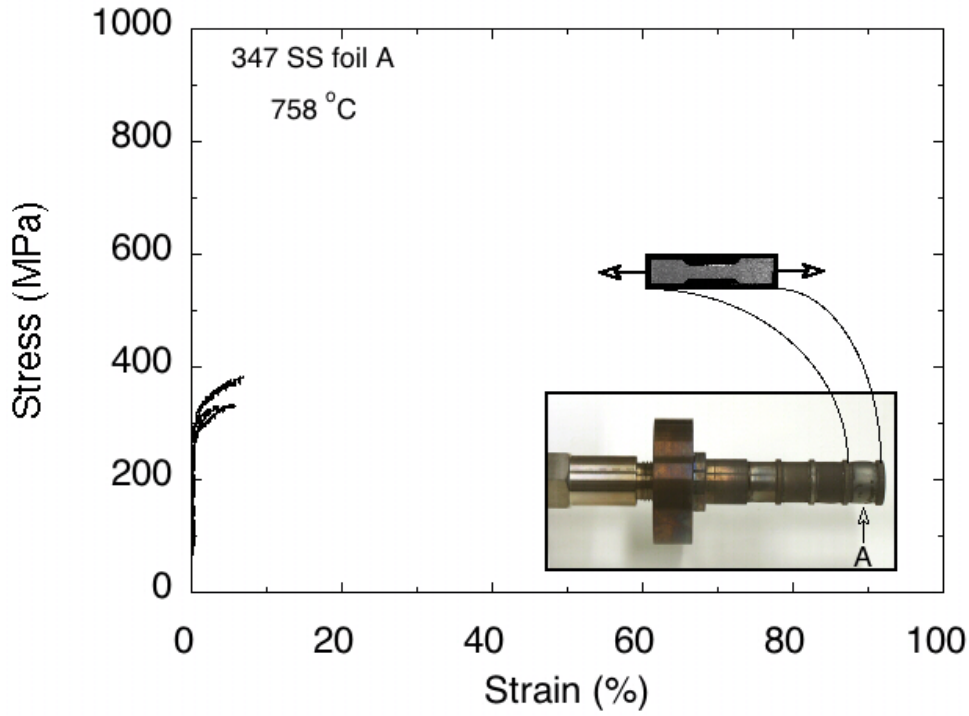

Figure 19. Stress-strain curves obtained from the tensile evaluation of miniature test specimens obtained from foil A (0.089-mm thick foil of 347 stainless steel) after 500-hr test.

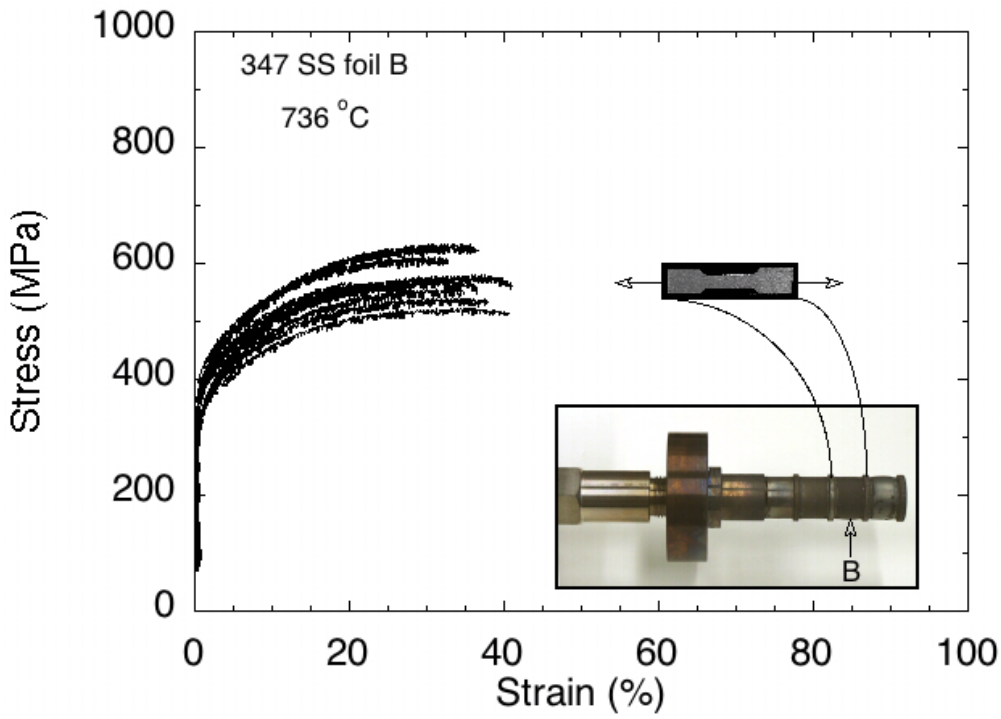

Figure 20. Stress-strain curves obtained from the tensile evaluation of miniature test specimens obtained from foil B (0.089-mm thick foil of 347 stainless steel) after 500-hr test.

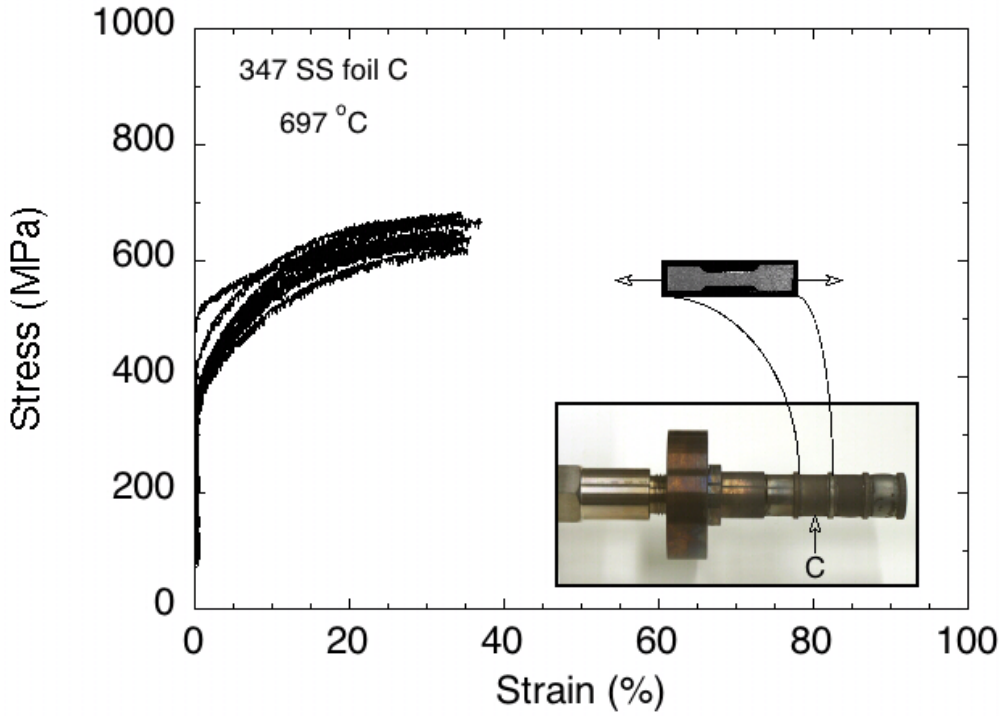

Figure 21. Stress-strain curves obtained from the tensile evaluation of miniature test specimens obtained from foil C (0.089-mm thick foil of 347 stainless steel) after 500-hr test.

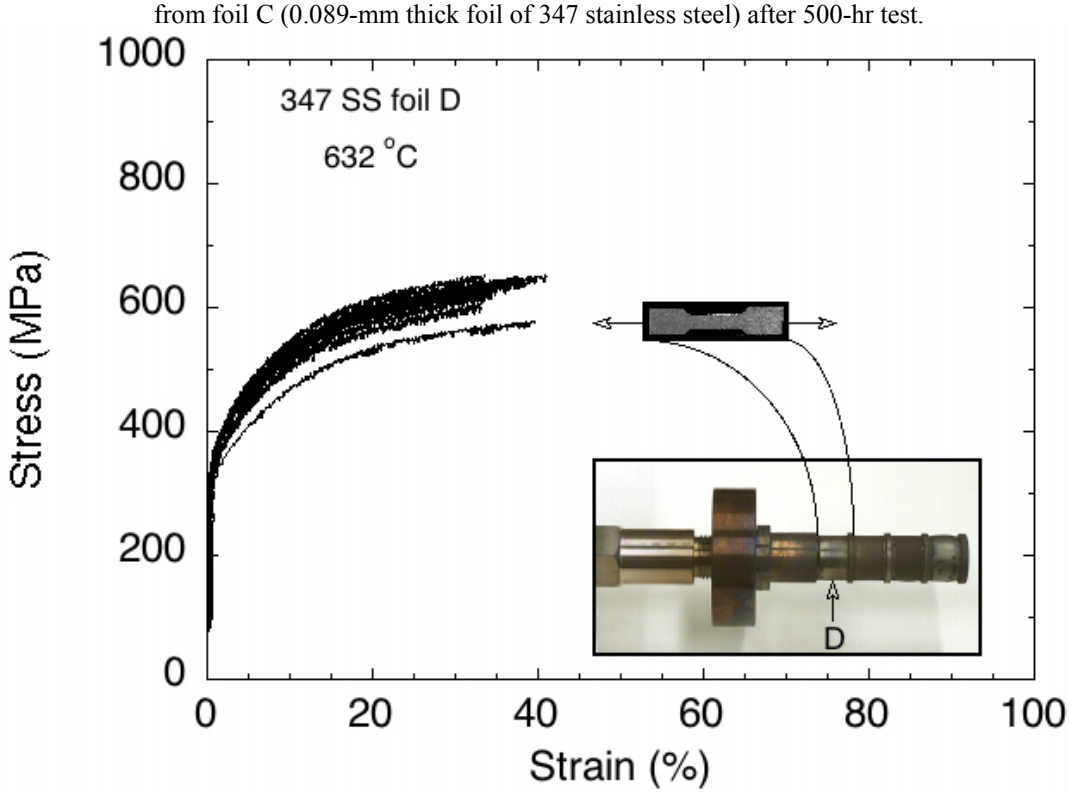

Figure 22. Stress-strain curves obtained from the tensile evaluation of miniature test specimens obtained from foil D (0.089-mm thick foil of 347 stainless steel) after 500-hr test.

The fracture surfaces of test specimens were analyzed by scanning electron microscopy. It was found, as illustrated in Figures 23 and 24, that fracture surfaces had dimples and

voids in the base metal, which are indicative of ductile failure. Although the residual ductility of foils B, C and D after 500-hr exposure was in excess of 20%, it was much less than the ductility of the as-processed material. The fracture surface of test specimens obtained from foil A also showed voids and dimples, but the features near the edge exposed to the exhaust gases were much coarser.

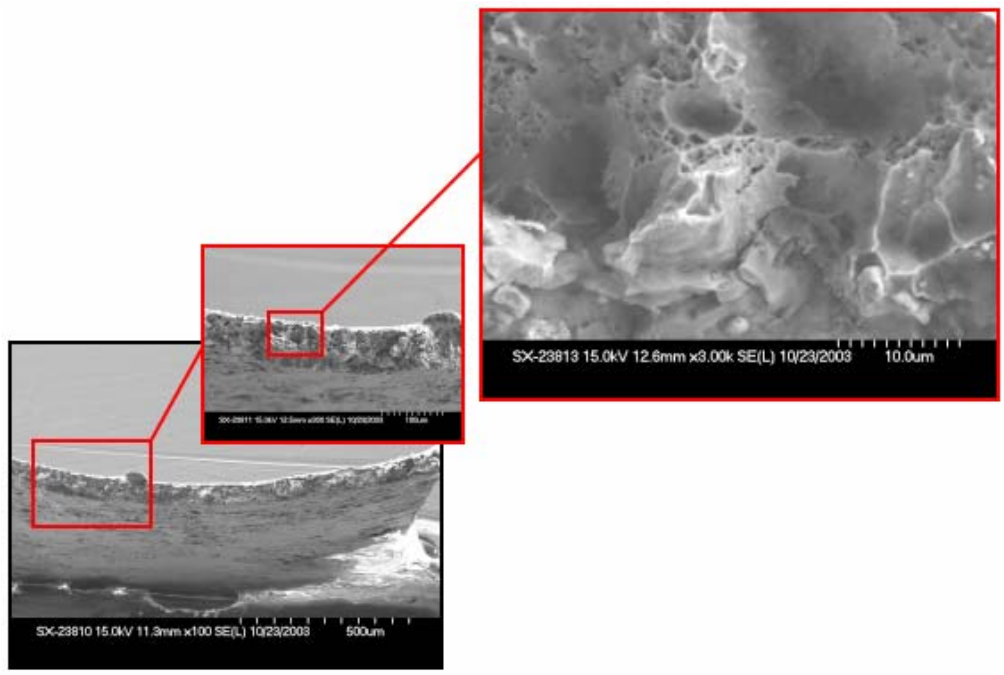

Figure 23. Scanning electron micrograph of fracture surface of foil A after 500-hr tests at 735°C and a tensile stress of 50 MPa. Although the material had experienced extensive corrosion, the base metal still exhibited ductile behavior.

Microstructural and chemical information from cross-sectional areas of the foils were obtained using an electron microprobe and backscattering scanning electron microscopy. Figure 25 shows scanning electron micrographs of cross-sectional areas obtained from foils A-D. The excessive oxidation of foil A is evident in these micrographs. As expected, the thickness of the oxide layer in these specimens increased with exposure temperature. Another important observation from the analysis of these micrographs is the asymmetry in the rate of corrosion of the material between the surface exposed to the exhaust gases and the surface exposed to air. The higher rate of corrosion on the surface exposed to the microturbine exhaust stream results from the interaction of water vapor and the oxide products that form on the surface of the material.

Elemental maps for chromium, iron, niobium, nickel and oxygen in a cross-section of foil A are presented in Figure 26. It can be observed that the base metal retains a uniform distribution of both iron and nickel, although the concentration of iron appears to be larger at the grain boundaries. Niobium appears to be randomly distributed in both the base metal, most likely in the form of sigma phase, and in the oxide layers.

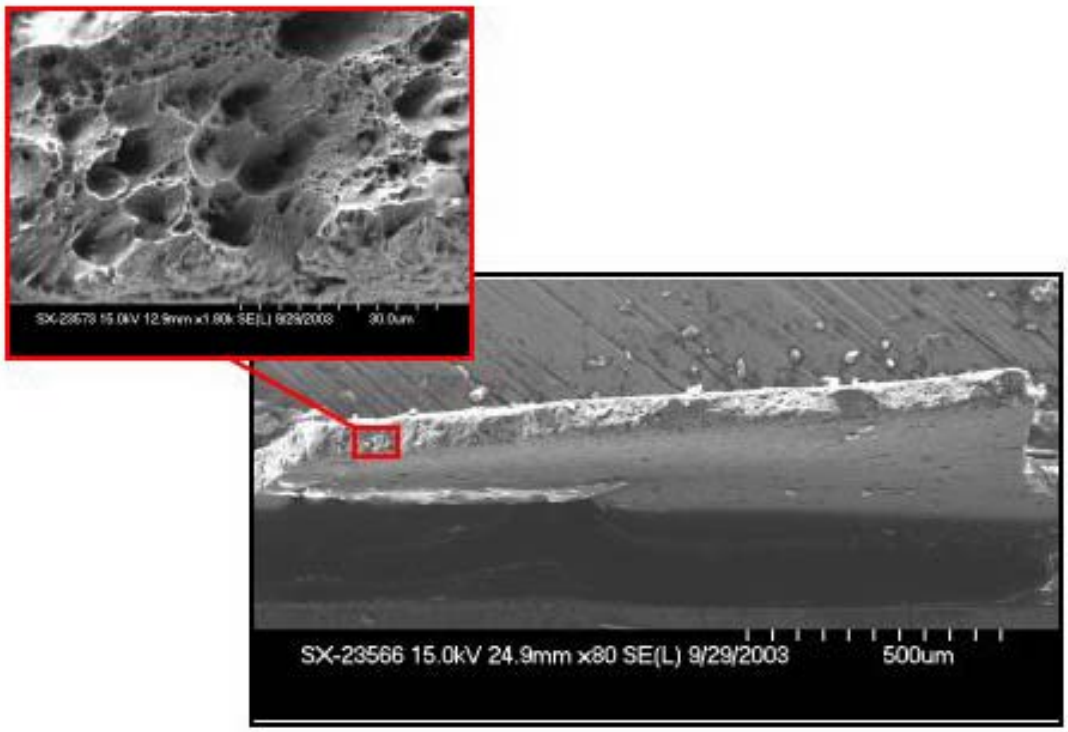

Figure 24. Scanning electron micrograph of fracture surface of foil B after 500-hr tests at 735°C and a tensile stress of 50 MPa.

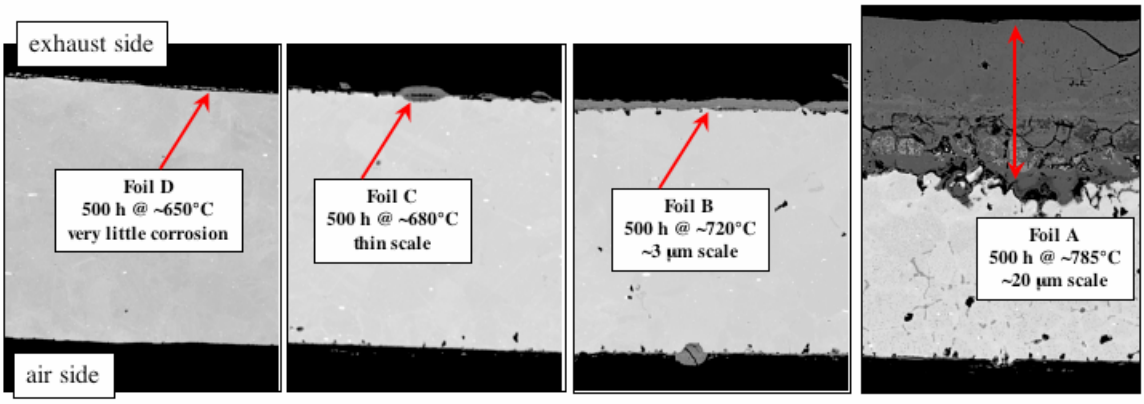

Figure 25. Scanning electron micrographs of cross-sectional areas of 0.089-mm thick foil of 347 stainless steel) after 500-hr test.

The concentration of chromium is highest in the oxide layer closest to the base metal and depletion of chromium from the grain boundaries in the base metal, particularly close to the metal-oxide interface is evident. The deficiency of chromium along these grain boundaries results from its diffusion to form a chromium oxide layer on the surface of the base metal. Above the chromium-rich oxide scale there appear to be two oxide scales. The first one contains nickel, chromium and oxygen, whereas the outermost oxide layer contains mostly iron and oxygen. Although the phases in these oxide scales were not

identified at this time, it is believe that the first two oxide scales consist of a layered structure of Cr_2O_3, $NiCr_2O_4$ and NiO [reference], while the outermost oxide layer consists of Fe_2O_3. The mechanisms leading to these phases will be investigated in collaboration with members of the Corrosion Science and Technology Group at Oak Ridge National Laboratory.

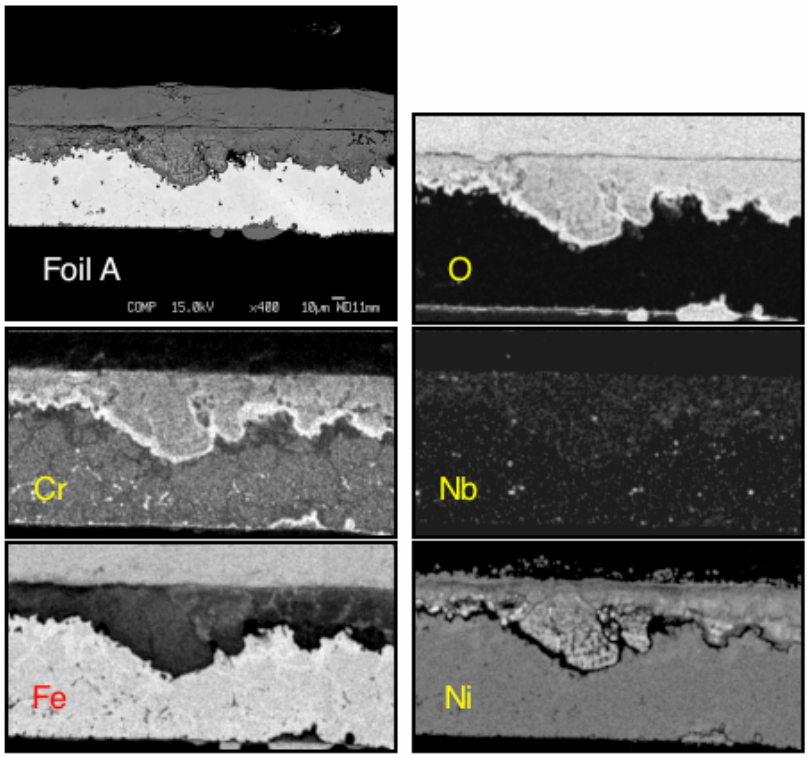

Figure 26. Elemental maps for cross-sectional area of Foil A after 500-hr test.

Table III. Summary of tensile properties of 0.089-mm thick foils of 347 stainless steel after 500-hr test at a TET of 800°C and tensile tangential stress of 50 MPa.

Foil	0.2% Yield Strength (MPa)	Ultimate Tensile Strength (MPa)	Failure strain (%)
A	310	351	4.9 ± 1.8
B	391	576	33 ± 6.6
C	410	647	35 ± 1.2
D	371	645	36 ± 2.8

Status of Milestones

On schedule

Industry Interactions.

The foils evaluated were graciously provided by Capstone Turbine Corporation.

Problems encountered

None

Publications/Presentations

None